DRAFT

Proceedings of IMECE 2007
2007 ASME International Mechanical Engineering Congress and Exposition
November 12-15, 2007 Seattle, Washington

IMECE2007-42937

3D MICROSTRUCTURE RECONSTRUCTIONS OF SOLID OXIDE AND PROTON EXCHANGE MEMBRANE FUEL CELL ELECTRODES WITH APPLICATIONS TO NUMERICAL SIMULATIONS OF REACTING MIXTURE FLOWS USING LBM

Bhavani V. Kasula [(a)], Leslie Mercado[(a)], Pietro Asinari [(b)], and Michael R. von Spakovsky [(a)]
[(a)] Center for Energy Systems Research, Mechanical Engineering Department,
Virginia Polytechnic Institute and State University,
Blacksburg, Zip Code VA 24061, U.S.A.
[(b)] Energy Engineering Department, Politecnico di Torino,
Corso Duca degli Abruzzi 24, Torino, Zip Code 10129, Italy

ABSTRACT

Computational modeling of fuel cell electrode-catalyst layers is an important tool in understanding the different electrochemical reactions and transport phenomena occurring within fuel cell electrodes. Proper modeling of this layer is required for an accurate prediction of cell behavior which in turn can be used for the development of more efficient fuel cells.

In macroscopic CFD approaches such layers are typically modeled as infinitely thin interfaces populated by sources and sinks or as very thin homogeneous porous layers. However, these layers are neither infinitely thin nor homogeneous and, thus, modeling in this fashion leads to a loss of information about the microstructure and its varying effects on the reacting mixture flows which pass through and into the structure. Thus, the utility of relying only on such macroscopic representations limits the general applicability of these macroscopic models as tools for design and for predicting fuel cell performance over a wide range of conditions. Furthermore, such macroscopic models cannot aid in the design of the electrode-catalyst layer itself. In order to address this latter point, a microscopic/mesoscopic modeling approach can be used, e.g., the Lattice Boltzmann Method (LBM), which models the reacting mixture flow through the porous microstructure of the electrode-catalyst layer. However, to do so requires reconstructing the porous geometry of this layer which can be done by using 2D microscopic images of cross-sections of the layer to generate 3D geometries from, for example, stochastic models which are relatively cost efficient and lead to similar structures with approximately the same characteristics of porosity, catalyst loading, three-phase boundaries, etc. as the original structure. Two such 3D reconstruction methods, i.e. one based on the granulometry law (one-point statistics) and the other on two-point statistics, are applied to a 2D SEM (scanning electron microscope) image of an SOFC electrode-catalyst layer and to the 2D SEM and TEM (transmission electron microscope) images for such a layer in a PEMFC. Results for these reconstructions are presented as are results for reacting mixture flow simulations through the two different reconstructed 3D SOFC structures using a 3D LBM approach. The development and application of a 3D LBM model for two-phase reacting mixture flows in PEMFC electrode-catalyst layer structures is in progress and will be reported in a future paper.

INTRODUCTION

The focus of this paper will be primarily on the dominant electrodes of solid oxide (SO) and proton exchange membrane (PEM) fuel cells, i.e. on the oxidation (anode) electrode of SOFCs and on the reduction (cathode) electrode of PEMFCs. To begin with, the anode electrode of a SOFC is a porous structure made up of nickel yttria-stabilized zirconia (Ni + YSZ). The electrolyte which interfaces with this electrode consists of yttrium-stabilized zirconia (YSZ). The electrochemical oxidation reaction which occurs at this electrode takes place at the so-called three-phase boundaries

(TPB) which are the interfaces between the electron conducting nickel, ion conducting YSZ, and the pores which allow for the transport of the gas species. Hydrogen diffusing through the pores on the anode side from the gas channels combines with a negatively charged oxygen ion (O^{2-}) traveling through the electrolyte from the cathode side as indicated by

$$H_2 + O^{2-} \rightarrow H_2O + 2e^- \quad (1)$$

In this oxidation reaction, H_2 forms a molecule of H_2O and releases a pair of electrons. The electrons, thus, generated are conducted through, for example, an external circuit to the cathode side where they combine with the oxygen diffusing through the porous cathode from the gas channel to generate O^{2-} as shown in

$$\frac{1}{2}O_2 + 2e^- \rightarrow O^{2-} \quad (2)$$

In a PEMFC, the anode and cathode are separated from each other via a proton-conducting polymer electrolyte membrane (Nafion™). The electrochemical reactions occur in the electrode-catalyst layers which are the layers separating the electrolyte and the gas diffusion layers. Each electrode-catalyst layer consists of carbon, platinum, and polymer. As in the SOFC, the electrochemical reactions take place at the TPB's which for the cathode electrode are the interfaces where the proton conducting polymer, electron conducting carbon, and the platinum catalyst come in contact with each other. In a PEMFC cathode electrode-catalyst layer, the oxygen not only flows through the pores but may as well diffuse through the polymer which contrasts with the SOFC anode electrode where the oxygen flow occurs only within the pores. Therefore, TPB's in the electrode-catalyst layers of the PEMFCs can be present even within the polymer material. The hydrogen oxidation reaction which occurs in the anode-catalyst layer produces protons and electrons, i.e.

$$H_2 \rightarrow 2H^+ + 2e^- \quad (3)$$

after which the protons pass through the electrolyte while the electrons are conducted through, for example, an external circuit to the cathode electrode-catalyst layer. In this layer, oxygen diffusing through this layer reacts with the protons and the electrons at the TPBs to produce water, i.e.

$$O_2 + 2H^+ + 2e^- \rightarrow H_2O \quad (4)$$

A number of 2D and 3D macroscopic models have been developed both for SOFCs and PEMFCs (e.g., [1-7]) in which the modeling of the electrodes when done as homogeneous layers requires the use of averaged parameters such as porosity, mean pore radius and tortuosity. All of these parameters vary from one microstructure to another and as such are limited in there ability to help distinguish the fundamental effects of electrode geometry on fuel cell performance.

Thus, modeling a fuel cell's electrode microstructure and the reacting flows which pass through them is an important task for properly understanding the complex phenomena of mass, heat, and charge transport as well as electrochemistry which occur in the electrodes during fuel cell operation. Factors such as the thickness of the electrode-catalyst layer, the porosity, pore connectivity, pore radius, and tortuosity affect the transport of the chemical species through the electrodes which in turn greatly influence the activation and concentration/ diffusive losses occurring on the cathode/anode sides of a fuel cell (e.g., see Lee et al. [8] and Chan et al. [9]).

One of the major problems in trying to do pore-scale modeling of the mass, heat, and charge transport in fuel cell electrodes is to numerically reconstruct the complex 3D porous microstructure of the electrodes or electrode-catalyst layers. Several reconstruction methods have been used in the literature in applications where there is only a single solid phase as opposed to the two solid phases in SOFCs or three solid phases in PEMFCs. One method combines a series of 2D sections to obtain a 3D structure. However, this is a difficult process which is limited by the impossibility of preparing sample cross sections with a spacing of less than 10μm [10]. Another possible approach is to use non destructive X-ray computed micro-tomography which directly produces a 3D pore space image at resolutions of around a micron [11]. But this resolution is not sufficient for reconstructing the electrode or electrode-catalyst layer microstructure which can have sub-micron size pores. One of the more popular ways of reconstruction is to stochastically reconstruct the 3D porous structure from microscopic 2D images of the porous microstructure [12-16]. This method is comparatively easy and cost efficient. These stochastic reconstruction methods can be applied to reconstructing SOFC and PEMFC electrode microstructures.

A primary focus of the present paper is a discussion and application of two stochastic modeling techniques for reconstructing fuel cell microstructures from 2D microscopic images obtained from scanning electron microscopy (SEM) and transmission electron microscopy (TEM). The two techniques used are

a) one-point statistics or the granulometry law method which takes into consideration the porosity of the medium and an assumption that the porous medium is made up of regular grains of a fixed known shape; and
b) two-point statistics which provides a more reliable reconstruction since it takes into account porosity and the two-point auto-correlation function which provides information about the connectivity of the pores in the porous medium.

To obtain the images for a PEMFC, a membrane electrode assembly was fabricated at the Center for Energy Systems Research at Virginia Tech and SEM and TEM images of electrode-catalyst layer cross-sections were taken. Images for the SOFC electrode cross-sections were obtained from the literature although efforts are currently underway to develop these images at facilities at the Politecnico di Torino.

The other primary focus of the present paper is to present results for the mesoscopic modeling of reactive mixture flows in reconstructed SOFC microstructures. The kinetic model,

which appears in [17-19], is used and solved via the lattice Boltzmann method (LBM), which is an alternative computational fluid dynamics approach for modeling fluid flows in complex geometries such as porous structures. In the present work, this model is used to study the gas species transport through the stochastically reconstructed SOFC porous anode electrodes generated by both one-point and two-point statistics.

STOCHASTIC RECONSTRUCTION

For the porous reconstruction, a microscopic 2D cross-sectional image is first converted into a digital binary image so that the geometrical parameters needed for microstructure reconstruction can be characterized. Figure 1a shows a sample SEM microscopic image of a PEMFC cathode catalyst layer while Figure 1b shows the digital binary image. This latter image is obtained from the former by thresholding, which is a process that differentiates between the solid phase and the pore phase by setting a limit on the intensity of the brightness in the image. The digital image is a binary image in which the solid phase is represented by 0's (black) and the pore phase by 1's (white).

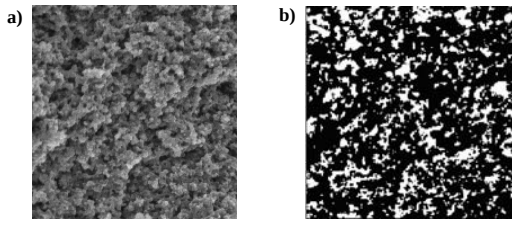

Figure 1. a) Original SEM image and b) digital image.

Characterization of the Geometric Parameters

The pore space of a porous medium is characterized by a phase function $Z(\mathbf{x})$ which is equal to 1 when $\mathbf{x}$ belongs to a pore space and 0 otherwise [14]. Here $\mathbf{x}$ denotes the position with respect to an arbitrary origin. The porosity and the two-point auto-correlation function are the first two statistical moments of the phase function. The porosity is the probability that a voxel, i.e. each elementary unit obtained by discretizing the 3D continuum space, is in the pore space and is given by

$$\varepsilon = \overline{Z(\mathbf{x})} \tag{5}$$

The two point auto-correlation function is the probability that two voxels separated by distance **u** are both in the pore space and is defined as

$$C(\mathbf{u}) = \overline{Z(\mathbf{x})Z(\mathbf{x}+\mathbf{u})} \tag{6}$$

Here the over bar denotes a statistical average and **u** is the lag vector between the two voxels. For a statistically homogeneous porous medium, the porosity, ε, is constant and the auto-correlation function, $C(\mathbf{u})$, is only a function of $\mathbf{u}$ and is independent of the location vector $\mathbf{x}$.

One-Point Statistic (Granulometry Law) Reconstruction

This method of porous reconstruction only takes into account the first statistical moment of the phase function, i.e. the porosity, ε, obtained from the 2D images. It is also based on the assumption that the porous medium is made up of grains of different sizes belonging to the solid phase. In 2D, the grains are defined as squares of different sizes which make up the porous image, while in the reconstructed 3D porous geometry, the grains are cubes of different sizes.

Once the digital image has been obtained, the granulometry law is applied to the image. The process involves counting how many grains, characterized by a given shape (square) and a given size, exist in the digital image. The procedure used to obtain the total number of grains of a particular grain size is as follows:

a) The whole digital image is checked for the largest grain size possible.
b) Wherever that particular grain size is obtained from the image, the corresponding cells are converted into neutral cells (i.e. they are no longer considered in the subsequent checks)
c) The total number of grains belonging to that particular grain size is counted.

The above procedure is repeated for the next largest grain size and so on until the total count for the least grain size is obtained. Figure 2 shows the possible distribution of the grains of different sizes but of the same shape (square) that can be present in a small cross-section of the digitized binary image. Grains of larger size are relatively few as opposed to smaller grains which occur in larger numbers.

The granulometry law, which is a relationship between the

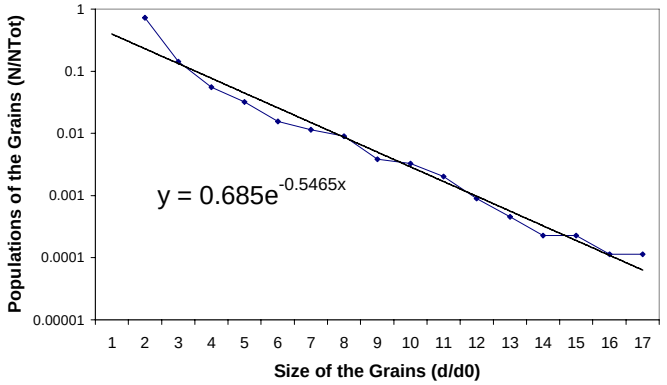

Figure 2. Granulometry law: relative populations corresponding to characteristic grain sizes.

grain size and its frequency for the solid phase is reasonably interpolated by the following expression:

$$\frac{N_i}{N_t} = 0.685\,exp\left(-0.5465\frac{d_i}{d_0}\right) \equiv f(d_i) \tag{7}$$

where N_i is the total number of grains of a grain size d_i, N_t the total number of grains of all sizes, d_i the characteristic grain size, and d_0 the minimum grain size determined by the resolu-

tion of the image considered.

The 3D reconstructed geometry should have the same porosity as that of the 2D image. Let π_{3D} be the porosity as calculated from the 2D image. Then the porosity in 3D can be defined as

$$\pi_{3D} = \frac{L^3 - V_0}{L^3} \tag{8}$$

where L is the dimension of the 3D domain being generated and V_0 the total volume of all the obstructions in 3D. However, V_0 is the sum of all the grains of different grain sizes in 3D, i.e.

$$V_0 = \sum_i {d_i}^3 N_{i_{3D}} \tag{9}$$

Now, in view of equation (7) for the 2D case, one can write for the 3D case that

$$N_{i_{3D}} = N_{t_{3D}} f(d_i) \tag{10}$$

where $N_{i_{3D}}$ is the total number of grains of size d_i in 3D, and $N_{t_{3D}}$ the total number of grains of all sizes in 3D. Combining equations (9) and (10) yields

$$V_0 = N_{t_{3D}} K \tag{11}$$

where $$K = \sum_i {d_i}^3 f(d_i) \tag{12}$$

Then from equations (8) and (11), the 3D porosity is given by

$$\pi_{3D} = \frac{L^3 - N_{t_{3D}} K}{L^3} \tag{13}$$

Now, the total number of grains of all sizes in 3D can be calculated as

$$N_{t_{3D}} = \frac{1 - \pi_{3D}}{\left(K / L^3 \right)} \tag{14}$$

Once these are known, the total number of grains corresponding to different grain sizes in 3D can be found using equation (10). This information is then used to generate a random porous structure as outlined in the procedure below.

a) The computational domain is first randomly filled with the largest sized grains possible.
b) Next, the computational domain is randomly filled with the next largest sized grains.
c) This procedure is continued till grains of the smallest size are filled into the computational domain.

Using this procedure, a porous geometry is reconstructed which has the same porosity as that of the microscopic image and is made up of cube shaped grains. Figure 3 shows the reconstructed porous image using granulometry law (one-point) statistics.

Two-Point Statistics Reconstruction

The reconstruction method based on two-point statistics makes use of the geometrical parameters, i.e. porosity and a two-point auto-correlation function. A petrographic analysis software called IMAGO, which is used in the petroleum industry, is employed here for the reconstruction using the two-point statistics. This software makes use of the Gaussian truncated method developed by Adler et al. [15] and Liang et al. [16] for the 3D reconstruction assuming homogeneity and isotropy. The 3D porous structure is created from 2D porous sections preserving the porosity and the auto-correlation function. Figure 4 shows the reconstructed geometry obtained using two-point statistics.

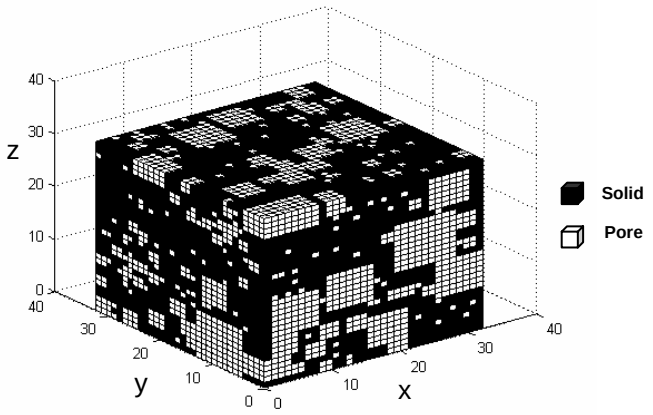

Figure 3. Porous geometry reconstructed using granulometry law.

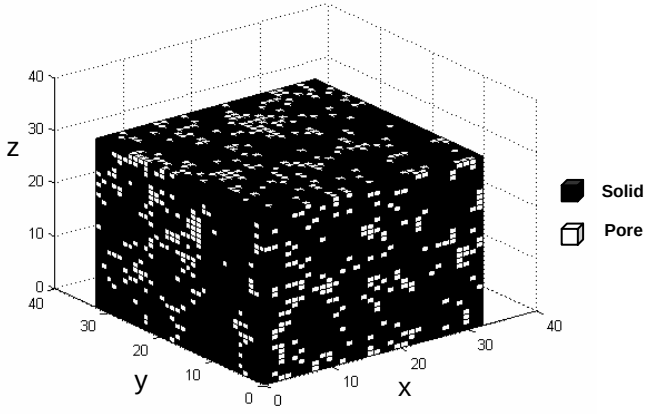

Figure 4. Porous geometry reconstructed using IMAGO.

SOFC ELECTRODE RECONSTRUCTION

The anode side electrode of a conventional electrolyte-supported planar SOFC is considered for the 3D reconstruction. The microscopic picture (seen in Figure 5) of a cross-section of the Ni-metal/YSZ-electrolyte electrode is obtained by means of back scanning electron microscopy [20]. The reconstruction is done both by the granulometry law (one-point) statistics and by using IMAGO for the two-point statistics.

3D Reconstruction of SOFC Using the Granulometry Law

In order to distinguish the two solid phases and the pore phase, a threshold operation is performed on the 2D microscopic image so that one can recognize the nature of the materials involved. Therefore, the original gray scale image is

converted into a digital image consisting of three different species. Figure 6a shows the original gray image and Figure 6b the digital image obtained.

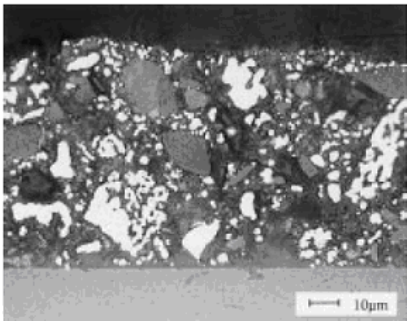

Figure 5. SEM microscopic image of the porous anode of the SOFC (bright: Ni; grey: electrolyte; black: pores).

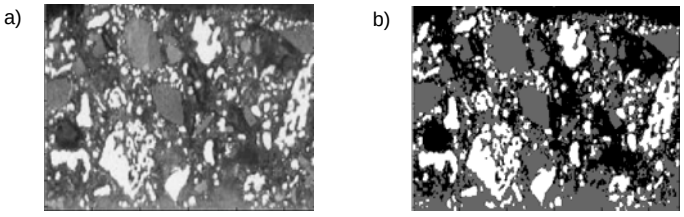

Figure 6. a) Original microscopic image and b) digital image.

Once the digital image is obtained, the granulometry law method as explained previously is applied to this image for each of the species (i.e. Ni and YSZ). In other words, the number of grains corresponding to a particular shape and size for each species is counted and the granulometry law is calculated for each species. Figure 7 shows the results for Ni and Figure 8 for YSZ.

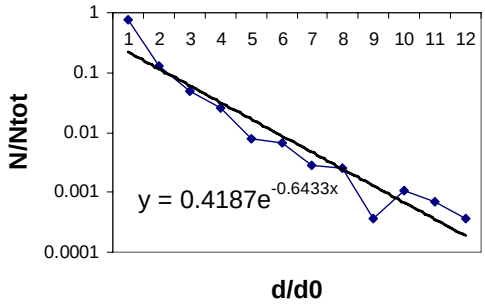

Figure 7. Granulometry law for Ni: relative populations with regards to the characteristic grain sizes for Ni.

The granulometry laws for both the species can be interpolated by the following exponential functions:

$$\left(\frac{N}{N_t}\right)_{Ni} = 0.4187\, exp\left(-0.6433\frac{d}{d_0}\right) \qquad (15)$$

$$\left(\frac{N}{N_t}\right)_{YSZ} = 0.2762\, exp\left(-0.6109\frac{d}{d_0}\right) \qquad (16)$$

where d_0 = 0.404 µm and is the minimum grain size considered and depends on the resolution of the micrograph.

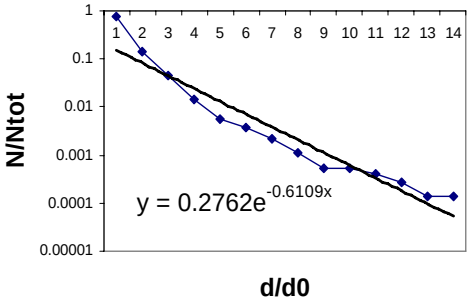

Figure 8. Granulometry law for YSZ: relative populations with regards to the characteristic grain sizes for YSZ.

Once the granulometry law correlation is found for each of the species, the total number of grains in 3D for each of the species can be used to calculate the grain distribution in 3D for both species. A code was developed in-house to do this and create a random porous structure for the SOFC anode layer.

Due to computational power restrictions, the size of the reconstructed geometry used for reacting mixture flow simulations may be different from the original image used for the 3D reconstructions. The thickness of the original image in the present case is around 80 µm so that ideally the thickness of the reconstructed image should be around 198 pixels. However, using a reconstructed image of this size is computationally challenging for the flow simulations. In order to ensure grid independent results, the computational mesh should be finer than the physical geometry which describes the porous geometry. For this reason, only a portion of the porous geometry reconstructed is actually used for the flow simulations so that large computational refinements can be considered which result in accurate estimations of the fluid flow. In particular, a 13 µm cube is considered which is filled by a 32^3 physical grid. Figure 9 shows the granulometry law (one-point) statistics based reconstructed 3D geometry used for flow simulations.

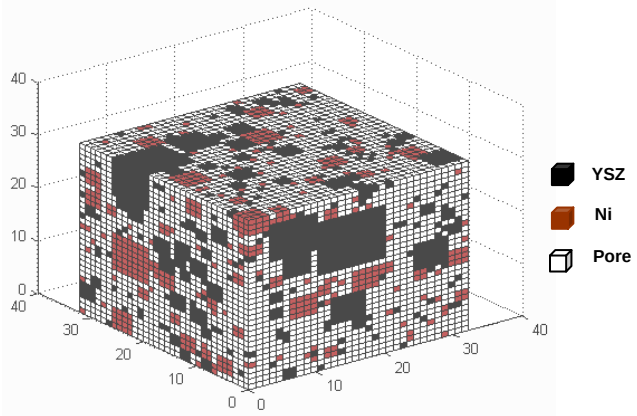

Figure 9. Reconstructed SOFC electrode layer with the one-point statistics.

3D Reconstruction of SOFC Using Two-point Statistic

Before applying the two-point statistics to reconstruct the SOFC anode layer in 3D, the thresholding operation is performed on the original micrograph (Figure 10a) so that an approximate distribution of Ni, YSZ and pores can be obtained. The threshold is selected such that the digital image for each species distribution is visually closer to the actual image. A better way of performing thresholding operation is to obtain the experimental values of the Ni and YSZ volume fractions and then apply the threshold which can result in a more accurate description of the distribution of the species. Work towards this is currently being performed at Politecnico di Torino and will be reported in a future work. Figures 10b),c),d) show the result obtained from thresholding. These digital images show the approximate distributions of the pore (Figure 10b)), YSZ (Figure 10c)), and Ni (Figure 10d)) distributions used as input images to the IMAGO software, which develops the volume fraction of the species or void fraction of the pores and the two-point auto-correlation function which gives the connectivity of the species or pores. Once these are known, IMAGO generates the 3D geometry for each species by the Gaussian truncated method. A code was developed in-house to combine the three geometries for Ni, YSZ, and the pores so that a final 3D SOFC porous anode geometry with appropriate volume fraction, porosity and species auto-correlation function is generated.

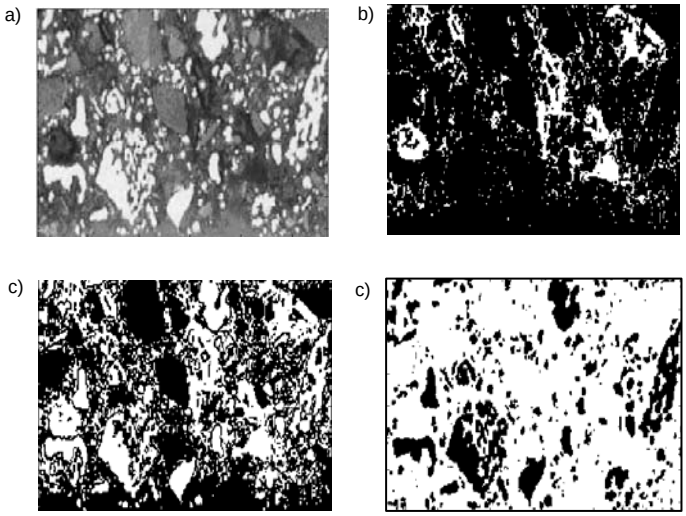

Figure 10. a) Original micrograph image (Ni: white; YSZ: gray; Black: pores); (b) digital image providing information about the pore distribution (white: pores); (c) digital image providing information about the YSZ distribution (black: YSZ); (d) digital image providing information about the Ni distribution (black: Ni).

In IMAGO, the resolution of the image is such that the size of each pixel is 0.3207 μm. The reconstructed geometry is a 10 μm cube which is considered to be filled with a 32^3 physical grid. Figure 11 shows the final reconstructed image of the SOFC anode using IMAGO.

PEMFC ELECTRODE CATALYST LAYER RECONSTRUCTION

The cathode side of a PEMFC electrode catalyst layer is considered for reconstruction. The membrane electrode assembly of a regular PEMFC is fabricated and SEM and TEM cross-sectional images are taken (see Figures 12 to 14). The SEM image in Figure 13 gives information about the distribution of the polymer within the porous structure. It does

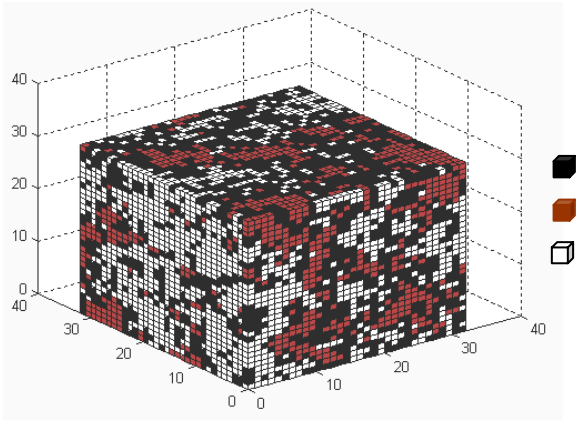

Figure 11. Reconstructed SOFC electrode with the two-point statistics.

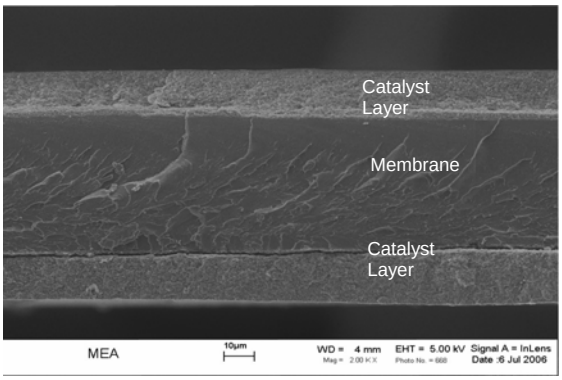

Figure 12. SEM cross-sectional image of the MEA.

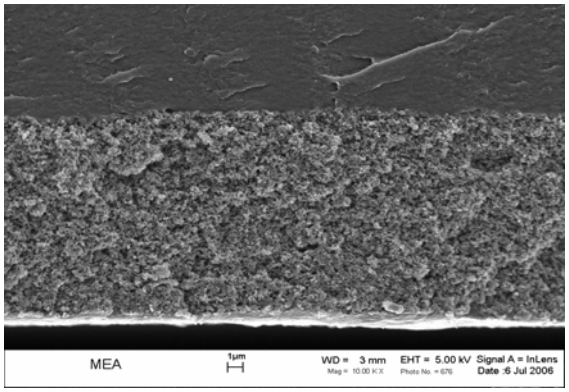

Figure 13. SEM image of the porous catalyst layer structure.

not provide any information about the distribution of the carbon and the platinum in this microstructure. This information, however, can be obtained from the high resolution TEM image (Figure 14) which is used for the catalyst layer reconstruction using the two-point statistics. The granulometry law (one-point) statistics, on the other hand, obtains this information from ex-

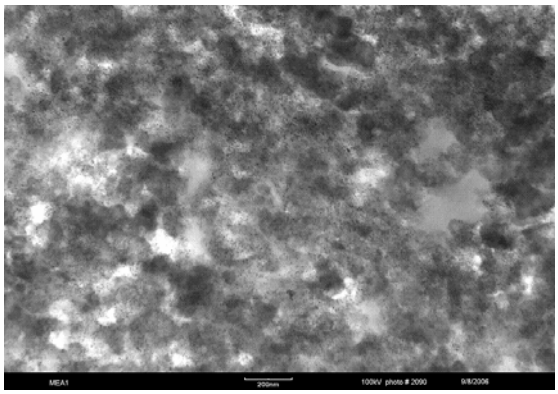

Figure 14. High resolution TEM image of the catalyst layer structure.

perimentally calculated values of the carbon and the platinum volume fractions in the porous structure, which are then used to randomly distribute these two species (phases) throughout the microstructure. A detailed description of the two different methods of PEMFC electrode catalyst layer reconstruction is given in the following sections.

3D Reconstruction of a PEMFC Electrode Catalyst Layer with the Granulometry Law (One-Point) Statistics

Figure 15a) shows the SEM PEMFC electrode catalyst layer portion used to obtain the granulometry law statistics. The porosity of the layer, the platinum catalyst volume fraction and the carbon volume fraction can be calculated experimentally during the fabrication of the membrane electrode assembly (MEA). A proper threshold is applied to the image shown in figure 15a so that the digital image has a porosity consistent with the experimentally calculated value. Figure 15b shows the digital image obtained from Figure 15a).

a) b)

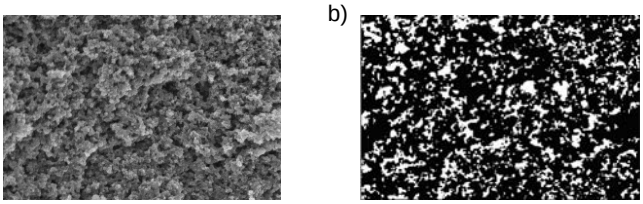

Figure 15. a) SEM PEMFC electrode catalyst layer image and b) generated digital image.

With this digital image, the number of grains corresponding per grain size is computed for the polymer phase. Figure 16 shows the results and the granulometry law obtained from this distribution is

$$\left(\frac{N_i}{N_t}\right)_{Polymer} = 0.685\, exp\left(-0.5465\frac{d_i}{d_0}\right) \qquad (17)$$

Here d_0 = 0.035 μm and is the minimum grain size considered. The thickness of the electrode catalyst layer is 14 μm which corresponds to 397 pixels in the SEM catalyst layer image and because of the flow computational restrictions mentioned above only a small portion of this layer is reconstructed, i.e. a cathode catalyst layer of 1.12 μm thickness is reconstructed and filled by a 32^3 physical grid.

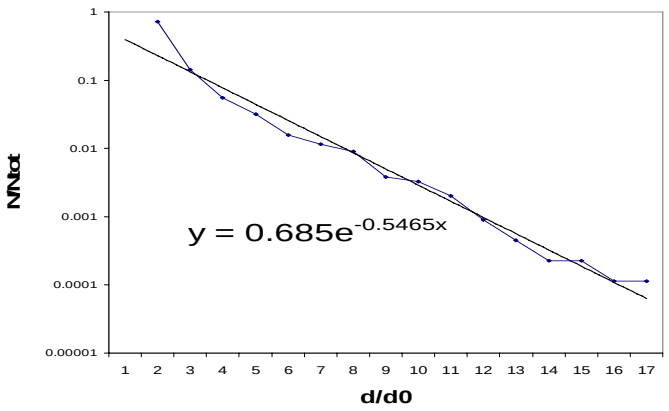

Figure 16. Granulometry law for the polymer.

With the granulometry law statistics for the polymer, the total number of grains in 3D for the polymer can be obtained and randomly distributed in the computational domain to generate a random porous structure consisting only of pores and the polymer phase. The porous structure obtained has a porosity similar to the experimentally calculated value but the polymer volume fraction is different since the solid portion of the regenerated structure has only the polymer phase and not the platinum and carbon phases. In order to be consistent with the experimentally calculated values of the volume fractions for the different phases, the polymer phase locations in the computational domain are randomly converted to carbon and platinum phases. Since in reality, the platinum particles are supported by carbon, care is taken that the platinum phases are in contact with the carbon phase. The final 3D reconstructed electrode catalyst layer geometry is shown in Figure 17.

3D Reconstruction of a PEMFC Electrode Catalyst Layer with the Two-Point Statistics

The two-point statistics reconstruction makes use of both the SEM and TEM images. The digital image obtained from the SEM image after thresholding operation gives the solid phase in the porous geometry. Using the porosity and the auto-correlation function obtained from this image, a 3D geometry is

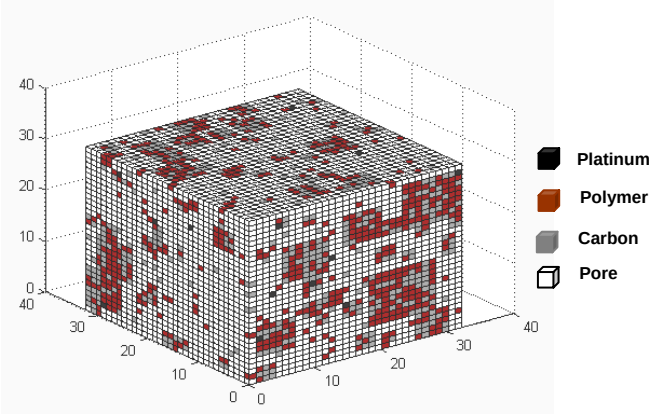

Figure 17. Reconstructed PEMFC cathode electrode-catalyst layer with one-point statistics.

generated using IMAGO. However, this generated geometry has only the polymer phase in it. To obtain information for the other two phases (platinum and carbon), the high resolution TEM image shown in Figure 14 is used. First, a threshold operation is applied on this image so that the digital image obtained from this TEM image has a carbon volume fraction similar to the experimental value. Figure 18a) shows the digital image for the carbon phase which is then used as input to IMAGO to generate a 3D geometry for this phase.

Another threshold operation is then performed on the TEM image for the platinum phase consistent with the volume fraction for platinum obtained experimentally. Figure 18b shows the digital image with the platinum phase, which is used by IMAGO to generate a 3D geometry consisting only of the platinum phase. A code developed in-house then combines the three different phase geometries into a single one. The final reconstructed 3D geometry obtained has a porosity and volume fractions of the polymer, carbon and platinum consistent with the experimental values. Figure 19 shows this reconstructed 3D geometry for the PEMFC electrode catalyst layer.

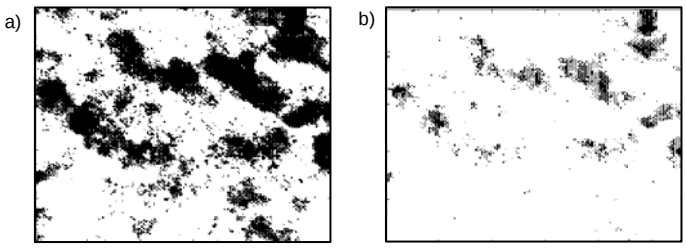

Figure 18. a) Digital image providing carbon phase information; b) digital image providing platinum phase information.

THREE-PHASE BOUNDARIES (TPBs)

Once the porous microstructure of the electrode catalyst layer has been reconstructed, the next step is to locate the three-phase boundaries (TPBs) present in the geometry. The procedure adopted is outlined in the following sections.

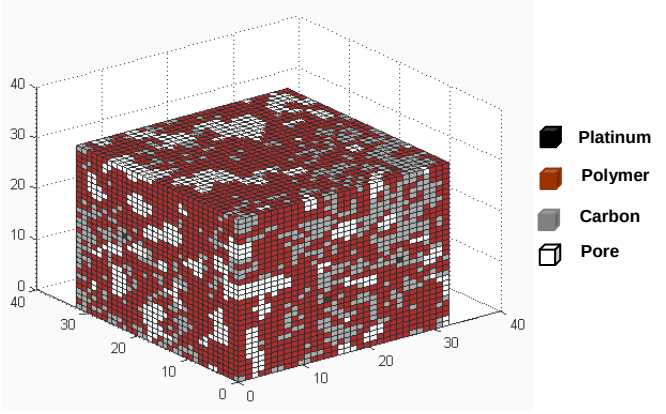

Figure 19. Reconstructed PEMFC cathode electrode-catalyst layer using two-point statistics.

Locating TPBs in the SOFC Electrode

In SOFC anode, the TPBs are the interfaces where the electron conducting nickel, ion conducting YSZ, and the gas transporting pores are in contact with each other. Thus, to identify the TPBs in the reconstructed geometry, one must check the locations where an electron conducting cell (i.e. Ni), an ion conducting cell (i.e. YSZ) and a gas transporting cell (i.e. pore) are in contact with each other. Also, for the electrochemical reaction to occur, there must be at least be one connection path for the electron conducting cell with the electron collecting metal grid on the anode side. Similarly, for the ion conducting cell, there must be at least one connection path with the ion conducting electrolyte and one connection path for the gas transporting cell to the gas channel. A code developed in-house is used to identify the TPBs existing in the reconstructed SOFC geometry based on the above conditions.

Locating TPBs in the PEMFC Electrode Catalyst Layer

In the PEMFC, in addition to the oxygen transport through the pores, oxygen can diffuse through the polymer. Therefore, the reaction sites not only exist near the pores but may also exist within the polymer enclosing the carbon supported platinum. In the PEMFC, the TPBs are the interfaces where a gas transporting pore, ion conducting polymer, and electron conducting carbon supported platinum are in contact as well as where an ion conducting and gas transporting polymer and electron conducting carbon supported platinum are in contact with each other. Care must be taken to check that the carbon supported platinum has a connection path with the electron collector on the cathode side, the ion conducting polymer has a connection path with the electrolyte and the pore is able to transport oxygen from the gas channel. A code developed in-house is used to identify the TPBs in the reconstructed PEMFC geometry based on the above conditions.

SOFC ELECTRODE: REACTIVE MIXTURE FLOW

Once the porous microstructure of the electrode-catalyst layer is numerically reconstructed, it can be used to describe the reactive mixture flow through it. To do so, the kinetic model

for binary reacting mixture flow found in [17-19] is solved using a parallel LBM code developed previously. Since at present the code is only applicable to gases, it is only used here with the SOFC reconstruction. Currently the code is being updated for two-phase reacting mixture flows in PEMFC electrode catalysts layers and results for these flows will be reported in a future work. For the present, the existing code is used to study reacting mixture flows in the two SOFC electrode geometries reconstructed using one- and two-point statistics.

NUMERICAL RESULTS

The reconstructed anode electrodes of SOFC are considered to be computational domains filled with a 32^3 physical grid. In order to ensure that the numerical results are mesh independent, the computational domain is refined, i.e. the computational mesh is denser than the physical grid. Therefore, the actual computational domain on which the calculation is done has 256^3 cells. Since the LBM code used is parallel in nature, this computational domain is decomposed and solved on 64 CPUs (nodes) of the massively parallel supercomputer, System X, at Virginia Tech. The typical domain decomposition for 64 CPUs is regular and is reported in Figure 20. It also shows the different gas species coming in and going out of the bottom plane which is the interface plane with the gas channel.

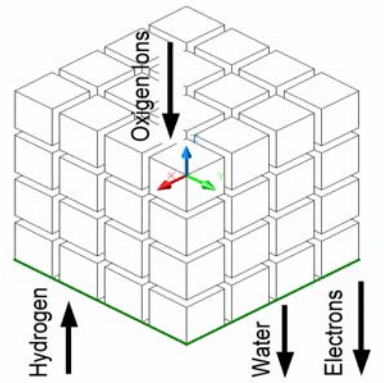

Figure 20. Schematic of the computational domain decomposed on 64 computational nodes. The species flow directions and the main input/output bottom plane are outlined.

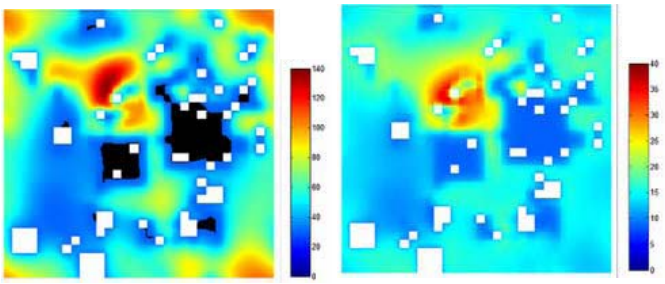

(a) $\left(\frac{\rho_{H_2O}\mathbf{u}_{H_2O}}{\rho_0 c_0}\right)$ (b) $\left(\frac{\rho_{H_2}\mathbf{u}_{H_2}}{\rho_0 c_0}\right)$

Figure 21. Normalized surface-averaged mass flux contours at the bottom plane for the SOFC reconstructed geometry with one-point statistics: a) outgoing mass flux contour of water produced; b) incoming mass flux contour of hydrogen consumed. (The normalization constants are $\rho_0 = 1\text{kg/m}^3$ and $c_0=3685\mu\text{m/s}$).

The electrochemical reactions do not occur in the bulk fluid but only at the TPBs where on the anode side, hydrogen is consumed and water produced. The electrochemical reaction locally modifies the species concentrations and produces a concentration driven flow. Asinari et al. [17-19] proposed a strategy to tune the reactive boundary conditions to model for a given current density. For the present numerical simulations, the reactive boundary conditions are tuned for a current density of 0.4 A cm^{-2} (typical for SOFCs). The mass flux contours at the main input/output bottom plane for both reconstructed geometries are reported in Figures 21 and 22.

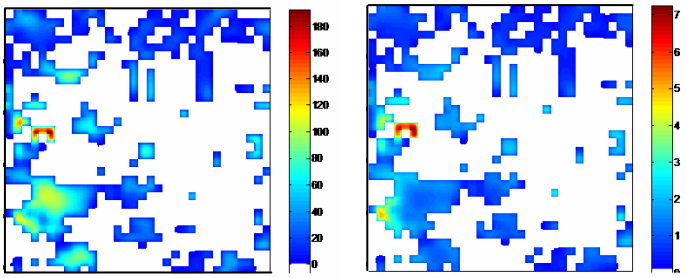

(a) Water (b) Hydrogen

Figure 22. Normalized surface-averaged mass flux contours at the bottom plane for the SOFC reconstructed geometry with two-point statistics: a) outgoing mass flux contour of water produced; b) incoming mass flux contour of hydrogen consumed.

Figure 21 shows the surface-averaged mass flux contours of the consumed and produced species at the bottom plane for the geometry reconstructed using one-point statistics. The black color represents the regions where the flux is reversed due to drag effect. The outgoing water produced due to the chemical reaction is reported in Figure 21a) and the incoming hydrogen which is consumed by the electrochemical reaction is shown in Figure 21b). Similarly, Figure 22 shows the surface-averaged mass flux of the produced water (Figure 22a)) and consumed hydrogen (Figure 22b)) at the bottom plane for the reconstructed geometry obtained from two-point statistics.

Figures 23 and 24 show the surface contours for mass fluxes of water and hydrogen at an intermediate plane for the one-point and two-point statistics reconstructed geometries. It can be seen from these contours that the maximum production of water and the maximum consumption of hydrogen are at the high reactive core, i.e. in those regions where there are more TPBs. In addition, it can be seen from these figures that there is a greater distribution of pores towards the outer bounds of the anode geometry generated with the one-point statistics than that generated with the two-point statistics (again for the same porosity). This means that there are fewer pores available within the geometry (at least at this intermediate plane) obtained using the one-point statistics than that using the two-

point statistics, resulting in fewer TPBs in the former than in the latter. Also the number of three phase boundaries may be higher in the two point statistics geometry than the one point statistics geometry due to the better connectivity between the pores and the different phases resulting from the use of the auto-correlation function which gives the connectivity between different phases. Thus, in general, it would appear that the two-point statistics based reconstruction may be a better reconstruction approach than that based on the granulometry law.

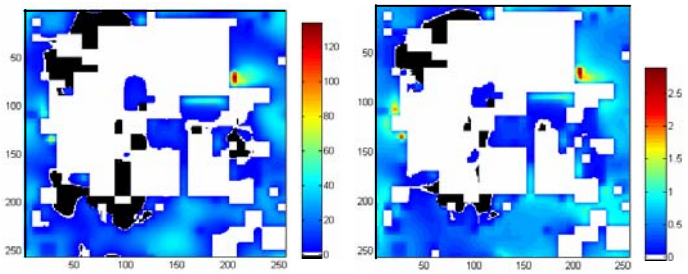

(a) Water (b) Hydrogen

Figure 23. Normalized surface-averaged mass flux contours at an intermediate plane for the SOFC reconstructed geometry with one point statistics. a) outgoing mass flux contour of water produced; b) incoming mass flux contour of hydrogen consumed.

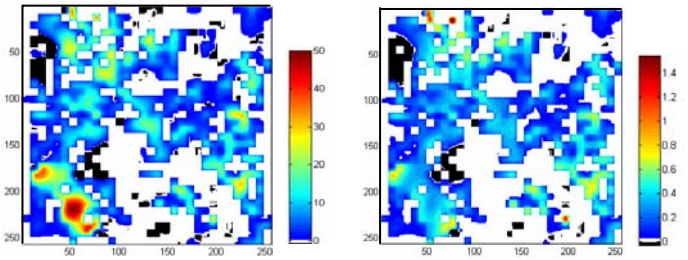

(a) Water (b) Hydrogen

Figure 24. Normalized surface-averaged mass flux contours at an intermediate plane for the SOFC reconstructed geometry with two point statistics. a) outgoing mass flux contour of water produced; b) incoming mass flux contour of hydrogen consumed.

Computation of Tortuosity

It has previously been shown that tortuosity is a fluid-dynamic concept that depends on the local fluid flows [17-19], i.e. the tortuosity depends on how a given species interacts with a particular porous medium[1]. As such, the tortuosity of water and hydrogen are not exactly the same since these two species follow different flow paths. Based on the methodology described in [17-19], the tortuosities are calculated for both the one-point and two-point statistics reconstructed geometries. The results are shown in Figure 25 where the surface-averaged tortuosities for the different species are given as a function of the normalized depth of the porous medium (electrode). In general, those for the two-point statistics are higher than for the one-point statistics.

In terms of the volume-averaged tortuosities, the results are reported in Table 2. As can be seen, the calculated numerical values for both the one-point statistics and two-point statistics

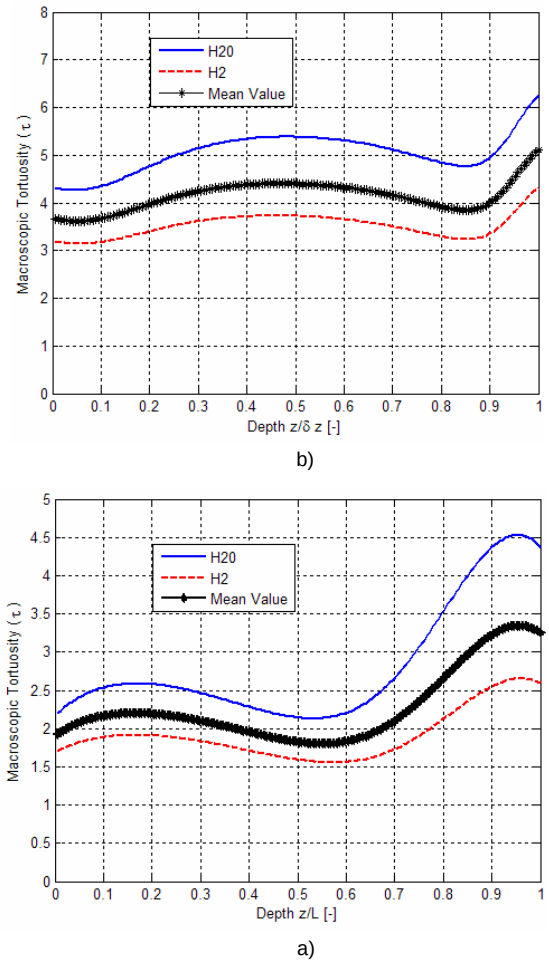

Figure 25. Surface-averaged tortuosity varying with normalized depth of the porous electrode for the a) one-point statistics reconstructed geometry and for the b) two-point statistics reconstructed geometry.

are reasonably close to the typical experimental value of 3 reported in [22] for characterizing SOFC anodes. This is an encouraging result in the sense that starting from only 2D microscopic images, one is able to stochastically generate 3D geometries which reasonably well match the volume-averaged tortuosities found experimentally.

[1] It is true that the tortuosity is usually considered to be a geometric parameter. However, it was originally introduced as a *kinematic property* equal to the average relative length of the flow path of a fluid particle from one side of a porous medium to the other [21]. If and only if a suitable model of the porous medium is chosen, e.g., one consisting of capillaries, then it also becomes a purely *geometric property*, since in this case, the fluid path is uniquely defined.

Table 2. Volume-averaged tortuosities computed for the different reconstructed geometries.

Reconstruction Method	Tortuosity
One-point statistics	2.2733
Two-point statistics	4.1420

Table 3 shows the volume averaged mass fluxes for water produced and hydrogen consumed for each of the reconstructed geometries. These volume-averaged mass fluxes are calculated for the entire volume in contrast to the contour plots of Figures 21 to 24 which only show surface area distributions for a given plane. It can be seen that the mass flux values in the geometry generated using one point statistics are more than the corresponding values for the two point reconstructed geometry. This is an interesting result as one would expect higher mass flux in the two point statistic geometry than in the one point statistic geometry because of the presence of the higher TPB's in the former. But this result can be attributed to the higher tortuosity in the two point statistic geometry which implies that there is a higher resistance to the flow of fluid in this geometry than in the one point statistic case.

Table 3. Normalized volume-averaged mass fluxes computed for the two different reconstructed SOFC anode geometries (for normalization constants refer to Figure 21).

Reconstruction Method	Water $\frac{\langle \rho_{H_2O}\mathbf{u}_{H_2O} \rangle}{\rho_0 c_0}$	Hydrogen $\frac{\langle \rho_{H_2}\mathbf{u}_{H_2} \rangle}{\rho_0 c_0}$
One-point statistic	10.5	3.92
Two-point statistic	6.88	2.12

CONCLUSIONS

Although both of the stochastic 3D reconstruction methods for SOFC electrodes and PEMFC electrode catalyst layers from 2D microscopic SEM/TEM images seem to be viable approaches, the method based on two-point statistics appears to result in a more realistic reconstruction of the microstructure. This conclusion is based both on the details of the methods (the two-point statistics incorporates more experimental data into its reconstruction approach) and on the results obtained from the numerical simulations for reacting mixture flows. The intention, of course, with both the reconstructions and flow simulations is to be able to eventually have a tool in which there is sufficient confidence that it can be used as a means for optimizing the designs of the electrode microstructures so crucial to fuel cell performance.

ACKNOWLEDGEMENTS

The authors would like to thank ESSS for their help and for providing access to the IMAGO™ software.

REFERENCES

[1] Ackmann, T., Haart, L. G. J., Lehnert, W., Thom, R.., "Modeling of mass and heat transport in thick-substrate thinelectrolyte layer SOFCs", Proceedings of the 4th European Solid Oxide Fuel Cell Forum, Lucerne/Switzerland, pp. 431-438, 2000.

[2] Li, P. W., Chyu, M. K., "Simulation of the chemical/electrochemical reactions and heat/mass transfer for a tubular SOFC in a stack" Journal of Power Sources, Vol. 124, no. 2, pp. 487-498, 2003.

[3] Springer, T., Zowodinski, T. and Gottesfeld, S., "Polymer Electrolyte Fuel Cell Model", Journal of the Electrochemical society, Vol. 138, pp. 2334-2341, 1991.

[4] Gurau,V., Liu, H. and Kakac, S., "Two-dimensional Model for Proton Exchange Membrane Fuel Cells", American Institute of Chemical Engineers Journal, Vol. 44, pp. 2410-2422, 1998.

[5] Coppo, M., Siegel, N. P., von Spakovsky, M.R., 2007, "On the Influence of Temperature on PEM Fuel Cell Operation," Journal of Power Sources, Elsevier Press, Vol. 159/1, pp 560-569, available on-line July 2006.

[6] Siegel, N. P., Ellis, M. W., Nelson, D. J., von Spakovsky, M. R., "A two-dimensional computational model of a PEMFC with liquid water transport", Journal of Power Sources, Vol. 128, no. 2, pp 173-184, 2004.

[7] Siegel, N. P., Ellis, M. W., Nelson, D. J., von Spakovsky, M. R., "Single domain PEMFC based on agglomerate catalyst geometry", Journal of Power Sources, Vol. 115, no. 1, pp. 81-89, 2003.

[8] Lee, J. H., Heo, J. W., Lee, D. S., Kim, J., Kim, G.H., Lee, H. W., Song, H. S., Moon, J. H., "The impact of anode microstructure on the power generating characteristics of SOFC", Solid State Ionics, Vol. 158, pp. 225-232, 2003.

[9] Chan, S. H., Khor, K. A., Xia, Z. T., "A complete polarization model of a solid oxide fuel cell and its sensitivity to the change of cell component thickness", Journal of Power Sources, Vol. 93, pp. 130-140, 2001.

[10] Dullien, F. A. L., "Porous media: Fluid transport and pore structure", Academic press, San Diego, 1992.

[11] Dunsmuir, J. H., Ferguson, S. R., D'Amico, K. L., Stokes, J. P., "X-ray microtomography- A new tool for the characterization of porous media, SPE 22860, Proceedings of the Annual Technical Conference, Dallas, Texas, October 6-9, pp. 423-430, 1991.

[12] Joshi, M., Ph.D. Dissertation, University of Kansas, Lawrence, KS, 1974.

[13] Quiblier, J. A., "A new three-dimensional modeling technique for studying porous media" Journal of Colloid Interface Science, Vol. 98, pp. 84-102, 1984.

[14] Adler, P. M., "Porous Media: Geometry and Transports", Butterworth-Heinemann, Stoneham, MA, 1992.

[15] Adler, P. M., Jacquin, C. G., and Quiblier, J. A., "Flow in simulated porous media", International Journal of Multiphase Flow, Vol. 16,no. 4, pp. 691-712, 1990.

[16] Liang, Z. R., Fernandes, C. P., Magnani, F. S., Philippi, P. C., "A reconstruction technique of 3-D porous media by using image analysis and using fourier transform", Journal of Petroleum Science and Engineering, Vol. 21, pp.273-283, 1998.

[17] Asinari, P., Calì Quaglia, M., von Spakovsky, M.R., and Kasula, B.V., 2007, "Direct Numerical Calculation of the Kinematic Tortuosity of Reactive Mixture Flow in the Anode Layer of Solid Oxide Fuel Cells by the Lattice Boltzmann Method", Journal of Power Sources, Vol. 170, pp. 359–375, 2007.

[18] Asinari, P., Quaglia, M. C., von Spakovsky, M. R., Kasula, B. V., "Numerical simulations of reactive mixture flow in the anode layer of solid oxide fuel cells by the Lattice Boltzmann method", Proceedings of ESDA, Torino, Italy. 4-7th July, 2006.

[19] Asinari, P., Coppo, M., von Spakovsky, M. R., Kasula, B. V., "Numerical simulations of gaseous mixture flow in porous electrodes for PEM fuel cells by the lattice Boltzmann method", proceedings of the "Third International Conference on Fuel Cell Science, Engineering and Technology", Ypsilanti, Michigan, 2005.

[20] Divisek, J., Volfkovich, Y., Wilkenhoener, R., "Structure investigations of SOFC anode cermets. Part I: Porosity investigations", Journal of Applied Electrochemistry, Vol. 29, pp. 153-163, 1999.

[21] Scheindegger, A. E., "The physics of flow through porous media", University of Toronto Press, 1960.

[22] Ackmann, T., Haart, L.G.J., Lehnert, W., Thom, F.,"Modeling of mass and heat transprot in thick-substrate thin-electrolyte layer SOFCs", Journal of the Electrochemical Society, Vol. 150, pp. 783-789, 2003.